

Four Faces of the Interaction between Ions and Aromatic Rings

Dóra Papp,^[a,b] Petra Rovó ^[c], Imre Jákli,^[d] Attila G. Császár ^{*,[a,b]} and András Perczel^{*,[d,e]}

Non-covalent interactions between ions and aromatic rings play an important role in the stabilization of macromolecular complexes; of particular interest are peptides and proteins containing aromatic side chains (Phe, Trp, and Tyr) interacting with negatively (Asp and Glu) and positively (Arg and Lys) charged amino acid residues. The structures of the ion–aromatic-ring complexes are the result of an interaction between the large quadrupole moment of the ring and the charge of the ion. Four attractive interaction types are proposed to be distinguished based on the position of the ion with respect to the plane of the ring: perpendicular cation– π (CP_{\perp}), co-planar cation– π (CP_{\parallel}), perpendicular anion– π (AP_{\perp}), and co-planar anion– π (AP_{\parallel}). To understand more than the basic features of these four interaction types, a systematic, high-level quantum chemical study is performed, using the $X^{-} + C_6H_6$, $M^{+} + C_6H_6$, $X^{-} + C_6F_6$, and $M^{+} + C_6F_6$ model systems with $X^{-} = H^{-}$, F^{-} , Cl^{-} , $HCOO^{-}$, CH_3COO^{-} and $M^{+} = H^{+}$, Li^{+} , Na^{+} , NH_4^{+} , $CH_3NH_3^{+}$, whereby C_6H_6 and C_6F_6 represent an

electron-rich and an electron-deficient π system, respectively. Benchmark-quality interaction energies with small uncertainties, obtained *via* the so-called focal-point analysis (FPA) technique, are reported for the four interaction types. The computations reveal that the interactions lead to significant stabilization, and that the interaction energy order, given in kcal mol⁻¹ in parentheses, is CP_{\perp} (23–37) > AP_{\perp} (14–21) > CP_{\parallel} (9–22) > AP_{\parallel} (6–16). A natural bond orbital analysis performed leads to a deeper qualitative understanding of the four interaction types. To facilitate the future quantum chemical characterization of ion–aromatic-ring interactions in large biomolecules, the performance of three density functional theory methods, B3LYP, BHandHLYP, and M06-2X, is tested against the FPA benchmarks, with the result that the M06-2X functional performs best. © 2017 Wiley Periodicals, Inc.

DOI: 10.1002/jcc.24816

Introduction

It is widely recognized that non-covalent interactions (NCI), such as hydrogen bonds, salt bridges, hydrophobic interactions, π – π stacking, and dispersion play a crucial role in determining the structure and even some of the functions of many complex molecular systems occurring in chemistry, biology, and material science. NCIs contribute to a range of phenomena related to the topic of molecular recognition, such as protein–ligand interaction, folding, crystal formation, solvation, and supramolecular self-assembly. Detailed understanding of the structural and energetic characteristics of NCIs is essential for the development of biomimetics and nanomolecular devices. NCIs are involved, for example, in enzymatic catalysis, as they may alter the configuration of an active site or stabilize the transition state of an enzymatic reaction. Furthermore, NCIs mediate protein–protein and protein–DNA interactions. While the relatively strong NCIs, for example, hydrophobic forces or H-bonds, control global folding, relatively weak interactions, for example, dispersion forces or π – π stacking, fine-tune the three-dimensional (3D) structure of proteins in a concerted manner, modulate folding efficacy, and this way enhance function and substrate selectivity.

Further NCIs, like interactions between ions and electron-rich π systems, including aromatic rings, have also been studied, often with a view on supramolecular biochemistry.^[1–12] The tunable physico-chemical properties of these ion–aromatic-ring (IAR) interactions have been exploited in the fields of drug design,^[13]

protein engineering,^[14,15] and host-guest chemistry.^[12] The IAR interactions offer improved selectivity, in some cases involving cooperative effects,^[16] which can facilitate the design of artificial ion transporters^[9] and sensors.^[17]

Aromatic moieties are often identified with strong hydrophobic interactions in the core of globular proteins or at protein–protein interfaces.^[18,19] Not only hydrophobic forces but also electrostatic interactions contribute to the bonding at

[a] D. Papp, A. G. Császár
MTA-ELTE Complex Chemical Systems Research Group, H-1518 Budapest
112, P.O. Box 32, Hungary
E-mail: csaszar@chem.elte.hu

[b] D. Papp, A. G. Császár
Laboratory of Molecular Structure and Dynamics, Institute of Chemistry,
Eötvös Loránd University, Pázmány Péter sétány 1/A, Budapest H-1117,
Hungary

[c] P. Rovó
Department Chemie und Pharmazie, Ludwig-Maximilians-Universität
München, Butenandstraße 5-11, Munich D-81377, Germany

[d] I. Jákli, A. Perczel
MTA-ELTE Protein Modeling Research Group, Institute of Chemistry, Eötvös
Loránd University, H-1518 Budapest 112, P.O. Box 32, Hungary
E-mail: perczel@chem.elte.hu

[e] A. Perczel
Laboratory of Structural Chemistry and Biology, Institute of Chemistry,
Eötvös Loránd University, Pázmány Péter sétány 1/A, Budapest H-1117,
Hungary
Contract grant sponsor: NKFIH; Contract grant numbers: K119658 (to
A.G.C.) and NK101072 (to A.P.)

© 2017 Wiley Periodicals, Inc.

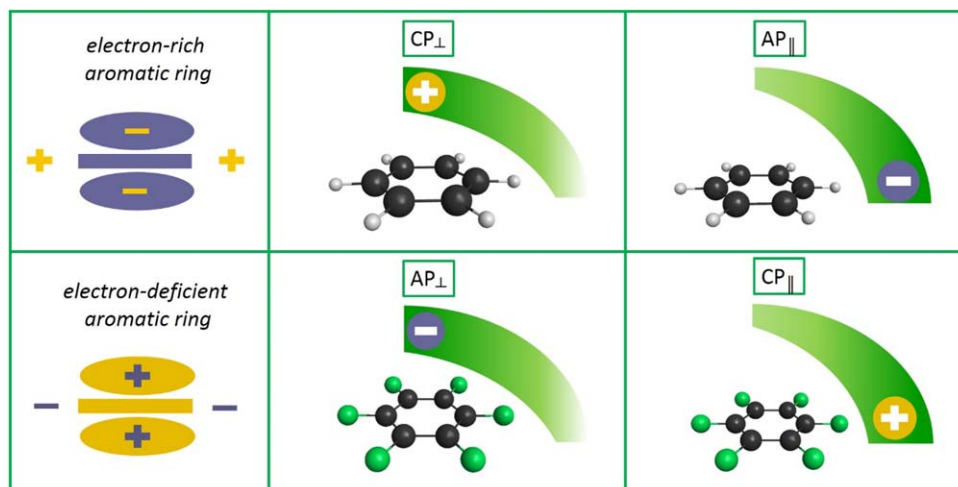


Figure 1. Schematic representation of the four types of interactions of ions with aromatic rings, based on the simple physical picture of quadrupole-charge forces. The carbon, hydrogen, and fluorine atoms are indicated in black, white, and green colors, respectively. The quadrupole moments of C_6H_6 and C_6F_6 are depicted in the top left and bottom left panels, respectively. The green bands of the rightmost four panels emphasize the assumed geometrical preferences of the four interaction types: the darker and broader the band the more preferred the position of the ion. [Color figure can be viewed at wileyonlinelibrary.com]

these sites. These interactions facilitate, for instance, the burial of charged side chains inside the hydrophobic core and the cation transport in channel membrane proteins.^[20] The simplest physical model of the IAR electrostatic interactions, forming the basis of the present study, uses the benzene (C_6H_6) and hexafluorobenzene (C_6F_6) molecules. Neither aromatic molecule, C_6H_6 as an electron-rich and C_6F_6 as an electron-deficient π system, has a dipole but C_6H_6 and C_6F_6 have similarly large negative and positive quadrupole moments,^[21] respectively (see the two leftmost panels of Fig. 1). Both model systems can thus readily interact with atomic charges or dipoles.^[21]

Based on the charge distribution and polarity of the aromatic system, we propose hereby to distinguish the following four attractive interaction types based on the position of the ion with respect to the plane of the ring: perpendicular cation- π (CP_{\perp}), co-planar cation- π (CP_{\parallel}), perpendicular anion- π (AP_{\perp}), and co-planar anion- π (AP_{\parallel}) (Fig. 1). As evident from Figure 1, the perpendicular cation- π and anion- π interactions are basically point-to-plane interactions, while the co-planar cation- π and anion- π interactions occur in an edge-wise fashion.

The most thoroughly studied quadrupole-charge interaction is the perpendicular cation- π interaction (CP_{\perp}).^[3,15,18,19] The CP_{\perp} interaction has been simply called cation- π interaction,^[2] but we advocate to call it CP_{\perp} , so that all four feasible IAR interaction types can be recognized straightforwardly. In proteins, the CP_{\perp} interaction generally occurs between the positively charged side-chain of Arg and Lys, or other charged moieties such as acetylcholine, and the π electron cloud of the electron-rich aromatic ring of the Phe, Tyr, or Trp amino acid residues.^[4] For instance, the CP_{\perp} interaction initiates gene expression in the nucleus when the Trp-rich aromatic cage of heterochromatin recognizes the trimethylated Lys of the protein histone.^[12] Over the past decades a number of experimental^[20] and theoretical^[22–26] studies attempted to quantify the strength of the CP_{\perp} interaction present in models of biomolecules. For example, Mecozzi et al.^[22,23] developed a simple, direct electrostatic model

that quantifies the binding energy associated with the formation of a metal-aromatic-ring complex. Mecozzi et al. emphasize that the perpendicular cation- π interaction is dominated by electrostatic contributions and that the variation in binding energies among different complexes can be rationalized by the change of the electrostatic potential around the aromatic ring.

The perpendicular anion- π interaction, AP_{\perp} , is the result of the attractive force between an anion and an electron-deficient aromatic system, such as C_6F_6 , trifluoro-triazine, 1,3,5-trinitrobenzene, and so forth.^[5,10,11] In analogy to CP_{\perp} , the AP_{\perp} interaction has traditionally been called an anion- π interaction. While the AP_{\perp} interaction is relatively rare in biological systems, it is quite common in supramolecular solid-state complexes.^[7] The specificity and selectivity of this NCI has been exploited in the design of artificial ion transporters,^[9] anion sensors,^[17] and receptors.^[27] Computational studies^[5,28–31] have demonstrated that the binding energy is dominated by electrostatic and anion-induced polarization contributions, and, similarly to the CP_{\perp} interaction, there is strong correlation between the magnitude of the quadrupole moment of the aromatic ring and the electrostatic contribution to the perpendicular anion- π interaction. This means that the larger the quadrupole moment the stronger the binding is. Based on high-level *ab initio* computations, Kim et al.^[30] established that the interaction energies of perpendicular anion- π complexes are comparable in magnitude to the corresponding perpendicular cation- π interactions. Interaction energies are presented for several perpendicular anion- π complexes by Mezei et al.^[31]

Complexes which exhibit a co-planar structural motif between an ion and an aromatic ring remained relatively unexplored.^[32–35] In proteins, the co-planar anion- π interaction has been associated with enzymatic activity, as demonstrated for ketosteroid isomerase, where in the active site the general base aspartate is situated next to two Phe side chains.^[34] Protein Data Bank (PDB)^[36] searches provided further evidence that negatively charged side chains, modelled by anions, show

geometrical preference for an edge-wise interaction with aromatic moieties. Thus, parallel anion- π interactions are expected to play a role in structure stabilization, ligand binding, and protein-protein interactions.^[32,33] The edge-wise interaction forces are expected to be weaker than the perpendicular (point-to-plane) ion- π ones; however, they exhibit larger spatial freedom, which can be advantageously utilized in supramolecular host-guest chemistry or in rational drug design.

To the best of our knowledge, the present study provides the first comprehensive and comparative analysis of all four possible interactions, CP_{\perp} , CP_{\parallel} , AP_{\perp} , and AP_{\parallel} , involving an aromatic ring and an ion. During the first step of our analysis, an extensive database search, involving PDB^[36] and the Cambridge Structural Database (CSD),^[37] is performed to reveal the significance of the four interaction types in macromolecules, including protein assemblies and organic and metal-organic complexes. After establishing the widespread occurrence of the four interaction types in a large number of complexes, we use electronic structure theory to clarify and prove the spatial preferences of the interaction types, as well as to reveal (quantum) effects underlying the structural characteristics. During the electronic structure computations we use the C_6H_6 and C_6F_6 molecules as models of ring-like aromatic species with opposite quadrupole moments, H^- , F^- , Cl^- , $HCOO^-$, and CH_3COO^- as anions, and H^+ , Li^+ , Na^+ , NH_4^+ , and $CH_3NH_3^+$ as cations. Due to the small size and/or high symmetry of the complexes, these model systems are ideal for high-accuracy quantum chemical computations. Next, based on the highly accurate interaction energies established for the four interaction types, we rank the interaction energies of ions with aromatic rings. The interaction energies, obtained via the sophisticated and thus expensive composite focal-point analysis (FPA) technique,^[38,39] serve as benchmark values for this and future studies. Finally, using these benchmark interaction energies as references, we realize another important goal of this study, when we test much less expensive density functional theory (DFT) methods whether they can reliably reproduce important interaction features, such as geometries and energetics, in larger IAR complexes.

Database Analyses

Motivated by earlier studies^[3,5,19,33,40] and the desire to start a comprehensive *ab initio* study only after finding sufficient experimental evidence for all four IAR interaction types, we carried out an exploratory database analysis involving the PDB^[36] and the CSD^[37] databases. We inspected the geometrical preferences of the CP_{\perp} , CP_{\parallel} , AP_{\perp} , and AP_{\parallel} interactions and tried to learn about their propensity in proteins as well as in small molecules. While database searches for the CP_{\perp} , AP_{\perp} , and AP_{\parallel} interactions have been performed before, for CP_{\parallel} we seem to provide here the results of the first database search.

CP_{\perp} and AP_{\parallel} interactions involving electron-dense aromatic rings were searched for in PDB. We constrained the analysis to amino acids having aromatic side chains, that is, Phe and Tyr, forming a complex with negatively charged amino acid residues, Asp and Glu. Competitive interactions, for example,

H-bonding, salt-bridge formation, and the presence of an oppositely charged ion, have been excluded from the search. As to AP_{\perp} and CP_{\parallel} interactions, which contain electron-deficient aromatic rings that are highly underrepresented in protein structures, we performed a search in the CSD. For the PDB analysis, we used a software developed previously in our group, while the CSD search was carried out using the ConQuest software.^[41] For the detailed description of the searching parameters, see the Supporting Information.

The database search results are summarized in Figures 2 and 3, corresponding to electron-rich and electron-deficient aromatic rings in PDB and CSD, respectively. The left panels of the figures depict the number of occurrences of IAR complexes as a function of what we call the plane angle, defined as the angle between the normal vector of the aromatic ring plane and the vector pointing from the centroid of the aromatic ring to one selected atom of the ion (details are given in the Supporting Information). The angle distributions reflect correctly the expected geometrical preferences arising from a quadrupole-charge interaction. The negatively charged ions are placed at the edge of the electron-dense aromatic ring of Phe or Tyr (AP_{\parallel} interaction), whereas cations tend to prefer a perpendicular structure in case of electron-rich aromatic rings (CP_{\perp} interaction) in proteins (Fig. 2). We can also observe that even the flexibility of a protein scaffold does not allow for a sharp distribution, due to the constraints of the given secondary and tertiary structures. Despite these restrictions, both the AP_{\parallel} and the CP_{\perp} interactions show clear geometrical preferences with a distribution maximum near 90° and 30° , respectively (Fig. 2).

To check whether the chosen structures correspond to the interactions sought, we plotted 3D coincidence diagrams, which show the plane angle and the distance ranges that our search covers simultaneously. From the 3D plots of Figure 2 (right-hand panels), it is clear that the maxima, as a function of the plane angle, correspond to a distance interval of $4.5 - 6.0 \text{ \AA}$ for the AP_{\parallel} interaction and $3.5 - 5.0 \text{ \AA}$ for the CP_{\perp} interaction. These intervals agree well with the expected interaction distances corresponding to these IAR complexes.

In Figure 3, the results of the CSD search are presented, involving electron-deficient aromatic rings and simple inorganic ions (the detailed list of search parameters is given in the Supporting Information). On the left panels of Figure 3, the distribution of the number of complexes shows clear preferences as a function of the plane angle. Anions are mainly located above an electron-deficient aromatic ring (AP_{\perp} interaction), while cations are located at the edge of an aromatic ring, indicated by a sharp peak (Fig. 3). Three-dimensional plots show a clear correspondence of angular and distance conditions, as the maxima in plane angle distributions correspond to an interval of $3.5 - 5.0 \text{ \AA}$ (AP_{\perp} interaction) and $6.0 - 7.0 \text{ \AA}$ (CP_{\parallel} interaction) in the distances.

To conclude, our database analysis supports the previously observed spatial preferences of IAR complexes and the PDB results clearly highlight the biological significance of IAR interactions. Moreover, the search in the CSD database confirms that the four interactions in the focus of this study occur even in less flexible small molecular complexes. However, one must

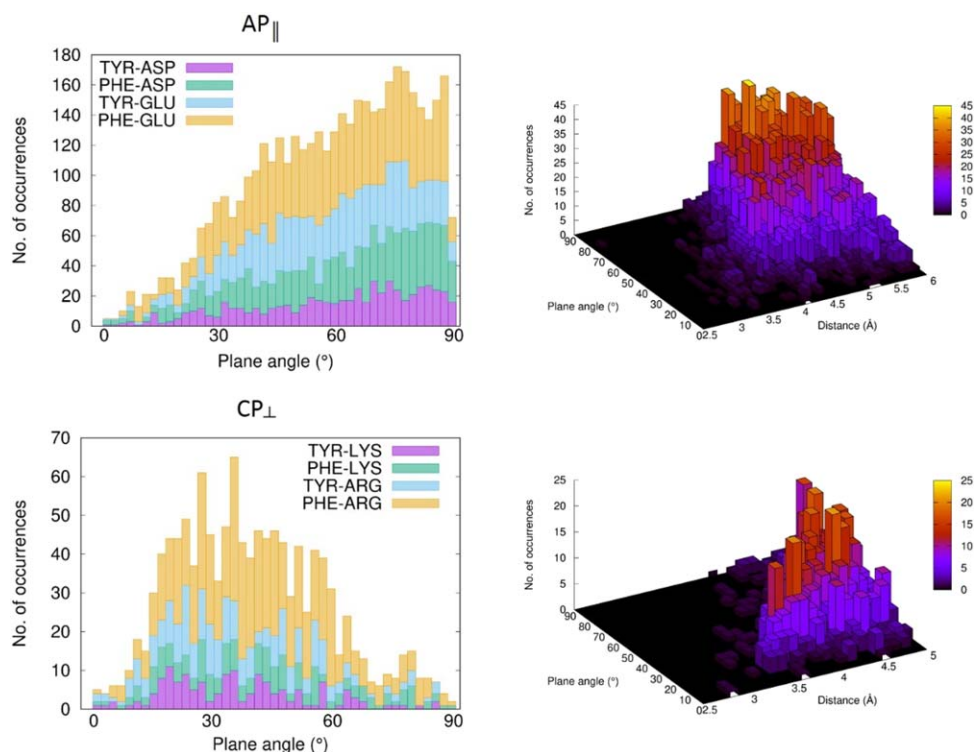


Figure 2. Based on a Protein Data Bank search, the left panels show the number of occurrences of ion–aromatic–ring (IAR) complexes for the two IAR interactions involving electron-rich aromatic rings as a function of the plane angle, defined as the angle between the normal vector of the aromatic ring plane and the vector pointing from the centroid of the aromatic ring to either an ion or a distinguished atom of a polyatomic ion. Different colors are used to depict different ion–aromatic–amino-acid complexes. Three-dimensional diagrams on the right-hand side show the coincidence of angular and distance conditions corresponding to the parallel anion- π ($AP_{||}$, upper panel) and the perpendicular cation- π (CP_{\perp} , bottom panel) interaction types. [Color figure can be viewed at wileyonlinelibrary.com]

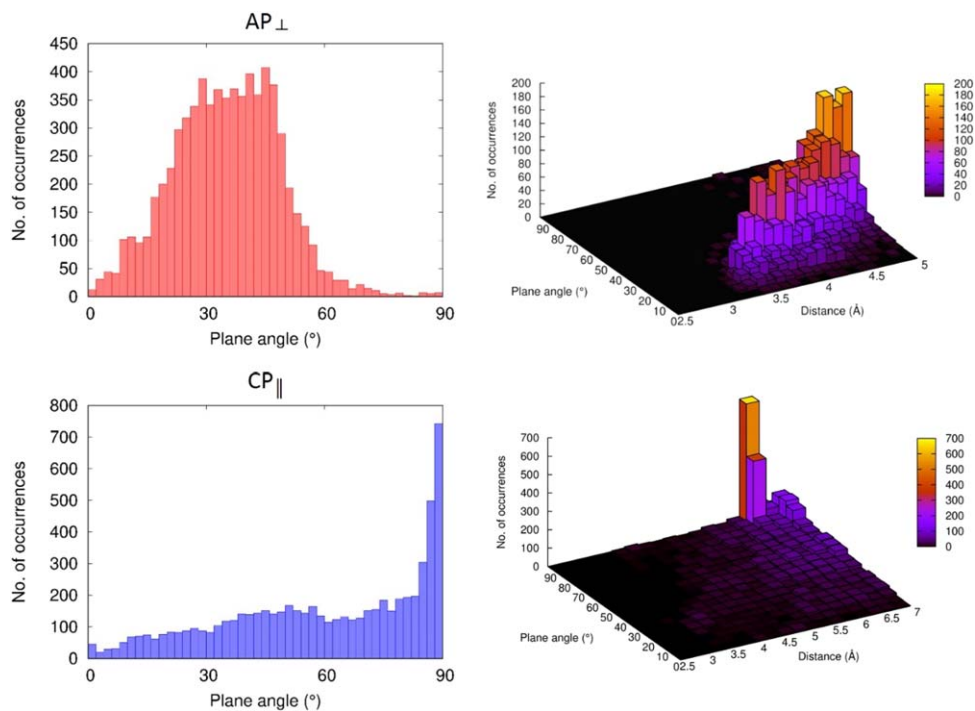


Figure 3. Based on a Cambridge Structural Database search, the left panels show, as a function of the plane angle defined as the angle between the normal vector of the aromatic ring plane and the vector pointing from the centroid of the aromatic ring to either an ion or one atom of a polyatomic ion, the number of occurrences of ion–aromatic–ring (IAR) complexes in the case of the two types of IAR interactions involving electron-deficient aromatic rings in small molecular complexes. The right-hand-side 3D diagrams show the coincidence of angular and distance conditions corresponding to the AP_{\perp} (upper panel) and $CP_{||}$ (bottom panel) interactions. [Color figure can be viewed at wileyonlinelibrary.com]

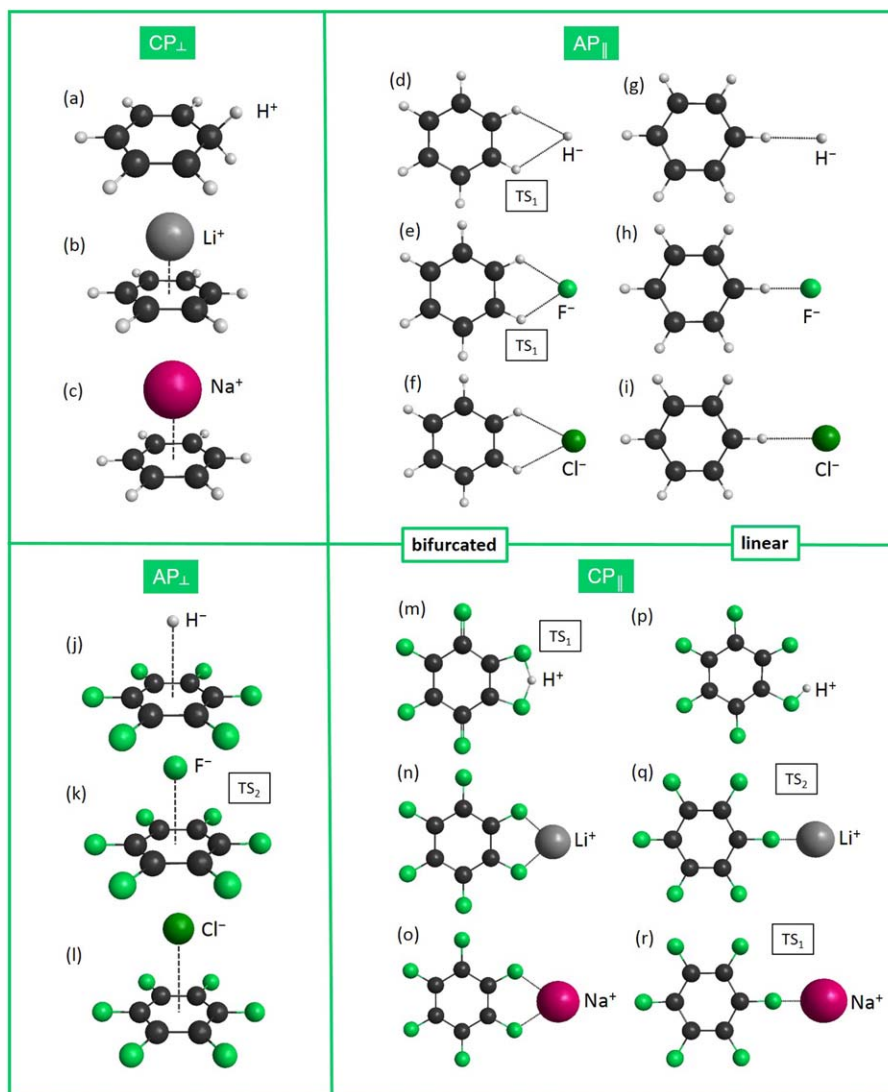


Figure 4. DF-MP2(FC)/aug-cc-pVTZ optimized structures of each ion–aromatic-ring complex, grouped according to the four basic interaction types (see Fig. 1). TS_n ($n = 1, 2$) refers to n th-order transition states on the potential energy surface of the given complex, the rest of the structures represent minima. Light grey, black, and light green spheres denote H, C, and F atoms, respectively. Solid lines are drawn from the ion to the molecule only in cases where the bonding is considered to be covalent. [Color figure can be viewed at wileyonlinelibrary.com]

note that dipole-dipole interactions may also play a significant role in real, less symmetric molecules, thereby altering the geometry and the relative energy of the interaction. Distance plots, reported in the Supporting Information, also reflect these conclusions, along with their strong dependence on the actual geometry and ion size. Deviations in the distance parameters from the expected values can be attributed to substituent effects or the interplay of various interactions in a macromolecule, and even solvation and steric repulsion may play an important role.^[40,42–44]

Advanced Techniques for the Quantitative and Qualitative Analysis of IAR Interactions

Focal-point analysis

The reference structures for the FPA analysis^[38,39] have been determined by geometry optimizations performed at the

frozen-core (FC) DF-MP2/aug-cc-pVTZ level of electronic structure theory, where DF-MP2 refers to density-fitted second-order Møller–Plesset perturbation theory^[45–47] and aug-cc-pVTZ is a triple-zeta member of the correlation-consistent atom-centered Gaussian basis set family of Dunning.^[48] In passing, we note that in a couple of cases, in particular in cases involving H^+ , the IAR interaction results in covalently bonded structures.

Using the DF-MP2(FC)/aug-cc-pVTZ reference structures, we performed a series of quantum chemical computations, required by the FPA scheme,^[38,39] to obtain benchmark-quality interaction energies characterizing each IAR interaction type. The FPA technique has provided highly accurate relative energies for several chemical systems, including peptide building blocks,^[49–51] amino acid complexes,^[52] and aromatic species.^[53] Within the FPA scheme^[38,39] it is usual to extrapolate the energies and the energy increments, computed at levels up to the coupled-cluster (CC) level of theory with single and double excitations including a perturbative estimate of

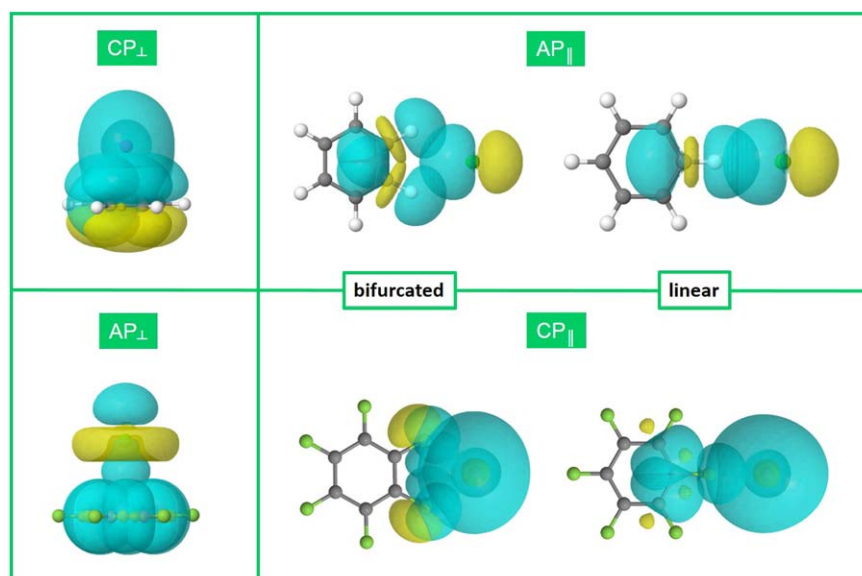


Figure 5. Stabilizing pre-orthogonal natural bond orbital overlaps characterizing the different ion–aromatic-ring interactions. The actual complexes considered are $\text{Na}^+ + \text{C}_6\text{H}_6$ (top left panel), $\text{Cl}^- + \text{C}_6\text{F}_6$ (bottom left panel), $\text{Cl}^- + \text{C}_6\text{H}_6$ (top right panel), and $\text{Na}^+ + \text{C}_6\text{F}_6$ (bottom right panel). [Color figure can be viewed at wileyonlinelibrary.com]

connected triple excitations (CCSD(T)), to the complete basis set (CBS) limit. FPA energies were computed in this study at the CCSD(T)/aug-cc-pVDZ, CCSD/aug-cc-pVXZ ($X = \text{D}, \text{T}$), and MP2(FC)/aug-cc-pVXZ ($X = \text{D}, \text{T}, \text{Q}$) levels of theory, where X is the cardinal number of the correlation-consistent basis set.^[48] For the electronic-structure computations the MOLPRO^[54] and GAUSSIAN09^[55] codes were used. The FPA scheme allows the estimation of the uncertainty of the interaction energies, and involves some so-called “small” corrections,^[39] such as the zero-point vibrational energy (ZPVE) and core-core and core-valence (abbreviated as “core”) electron-correlation corrections. The ZPVE corrections were approximated using the harmonic-oscillator model at the DF-MP2(FC)/aug-cc-pVDZ level, while the core corrections were estimated at the MP2/aug-cc-pCVTZ level. While in few-atom systems, it is usual to consider relativistic and diagonal Born–Oppenheimer correction contributions to relative energies, these corrections were deemed to be insignificant^[49,51,56,57] for this study to consider.

Natural bond orbital analysis

The natural bond orbital (NBO) analysis technique^[58,59] was applied to interpret the different types of interactions emerging in IAR complexes. The NBO analysis was performed at the HF/aug-cc-pVDZ level, where HF stands for Hartree–Fock. The NBO analysis yields overlaps between so-called pre-orthogonal natural bond orbitals (PNBOs).^[60] These overlapping orbitals can be visualized straightforwardly and allow a deeper qualitative characterization of the nature of the IAR interactions.

Variations on the Theme of Quadrupole-Ion Interactions

Electron-rich aromatic rings

The quadrupole moment of an electron-rich aromatic ring (Fig. 1, represented by benzene), according to the simple electrostatic

picture, directs a positive point charge into a “perpendicular” arrangement, whereby the positive charge sits on the top (or bottom) of the aromatic ring. In contrast, a negative point charge finds its optimum position in the plane of the ring, where it is attracted by a partial positive charge (Fig. 1). Based on this simple electrostatic picture, the most stable arrangements of the selected ions, H^- , F^- , Cl^- and H^+ , Li^+ , Na^+ , with respect to a benzene ring can be determined by scanning the hypothetical green band sketched in Figure 1. The coplanar arrangement can either be linear or bifurcated, as indicated in the two rightmost panels of Figure 4. Pictorial representation of the interacting PNBOs is shown in the upper two panels of Figure 5, based on optimized structures of the IAR complexes.

The interplay of attractive and repulsive orbital overlaps establishes the structure of an IAR complex. Repulsive forces emerge between two (or more) occupied orbitals. Stabilization always occurs through donor-acceptor interactions, that is, overlaps between empty (electron-acceptor) and electron-rich (electron-donor) orbitals. For instance, in the case of the CP_\perp interaction, the C–C bonding orbitals of the benzene ring (the six p -type orbitals originally belonging to each C atom of benzene, perpendicular to the plane of the ring, commonly referred to as the π -cloud) serve as electron donors, while the vacant valence-shell orbitals of the cation accept these electrons. In contrast, the AP_\parallel interaction is the result of overlaps between antibonding orbitals of the C–H bonds of benzene, two in the bifurcated and one in the linear case, and a lone pair of the anion. The interaction is particularly strong with a p -type lone pair of the chloride ion.

Electron-deficient aromatic rings

Using the simple electrostatic model of quadrupole-charge interaction, an electron-deficient aromatic ring directs charges just the opposite way as the electron-rich one does (see Fig. 1).

Table 1. Focal-point analysis of the interaction energies, in kcal mol⁻¹, of the Na⁺-benzene cationic complex, characterized by a perpendicular structure, and of the Cl⁻-benzene anionic complex, characterized by a co-planar structure with a bifurcated as well as a linear arrangement.

Na ⁺ -C ₆ H ₆ complex	$\Delta E_e(\text{HF})$	$\delta[\text{MP2}]$	$\delta[\text{CCSD}]$	$\delta[\text{CCSD(T)}]$	$\Delta E_e[\text{CCSD(T)}]$
aug-cc-pVDZ	-24.38	+1.14	-0.10	+0.04	-23.30
aug-cc-pVTZ	-23.62	+1.06	-0.22	[+0.04]	[-22.73]
aug-cc-pVQZ	-23.57	+1.25	[-0.22]	[+0.04]	[-22.50]
CBS	[-23.57(3)]	[+1.39(10)]	[-0.22(10)]	[+0.04(2)]	[-22.35(20)]
Extrapolation	$E_{\text{CBS}}^{\text{HF}} + \alpha(X+1)e^{-9\sqrt{X}} (X=3, 4)$	$E_{\text{CBS}} + bX^{-3} (X=3, 4)$	Additive	Additive	Additive
$\Delta E_{\text{final}} = \Delta E_e[\text{CCSD(T)/CBS}] + \Delta_{\text{core}}[\text{MP2/aug-cc-pCVTZ}] + \Delta_{\text{ZPVE}}[\text{DF-MP2(FC)/aug-cc-pVDZ}] = -22.35 - 2.21 + 1.14 = \mathbf{-23.42(25) kcal mol^{-1}}$					
Cl ⁻ -C ₆ H ₆ complex	$\Delta E_e(\text{HF})$	$\delta[\text{MP2}]$	$\delta[\text{CCSD}]$	$\delta[\text{CCSD(T)}]$	$\Delta E_e[\text{CCSD(T)}]$
Bifurcated structure					
aug-cc-pVDZ	-4.71	-4.46	+0.88	-0.76	-9.05
aug-cc-pVTZ	-4.35	-4.70	+1.07	[-0.76]	[-8.74]
aug-cc-pVQZ	-4.31	-4.52	[+1.07]	[-0.76]	[-8.52]
CBS	[-4.31(1)]	[-4.40(6)]	[+1.07(10)]	[-0.76(10)]	[-8.39(15)]
Extrapolation	$E_{\text{CBS}}^{\text{HF}} + \alpha(X+1)e^{-9\sqrt{X}} (X=3, 4)$	$E_{\text{CBS}} + bX^{-3} (X=3, 4)$	Additive	Additive	Additive
$\Delta E_{\text{final}} = \Delta E_e[\text{CCSD(T)/CBS}] + \Delta_{\text{core}}[\text{MP2/aug-cc-pCVTZ}] + \Delta_{\text{ZPVE}}[\text{DF-MP2(FC)/aug-cc-pVDZ}] = -8.39 - 0.17 + 0.02 = \mathbf{-8.54(21) kcal mol^{-1}}$					
Linear structure	$\Delta E_e(\text{HF})$	$\delta[\text{MP2}]$	$\delta[\text{CCSD}]$	$\delta[\text{CCSD(T)}]$	$\Delta E_e[\text{CCSD(T)}]$
aug-cc-pVDZ	-4.69	-4.08	+0.75	-0.71	-8.73
aug-cc-pVTZ	-4.41	-4.21	+0.94	[-0.71]	[-8.39]
aug-cc-pVQZ	-4.36	-4.01	[+0.94]	[-0.71]	[-8.14]
CBS	[-4.35(1)]	[-3.87(7)]	[+0.94(10)]	[-0.71(10)]	[-7.99(16)]
Extrapolation	$E_{\text{CBS}}^{\text{HF}} + \alpha(X+1)e^{-9\sqrt{X}} (X=3, 4)$	$E_{\text{CBS}} + bX^{-3} (X=3, 4)$	Additive	Additive	Additive
$\Delta E_{\text{final}} = \Delta E_e[\text{CCSD(T)/CBS}] + \Delta_{\text{core}}[\text{MP2/aug-cc-pCVTZ}] + \Delta_{\text{ZPVE}}[\text{DF-MP2(FC)/aug-cc-pVDZ}] = -7.99 - 0.17 + 0.14 = \mathbf{-8.02(23) kcal mol^{-1}}$					
The symbol δ denotes the increment in the relative energy (ΔE_e) with respect to the preceding level of theory in the hierarchy HF \rightarrow MP2 \rightarrow CCSD \rightarrow CCSD(T). Square brackets signify results obtained from basis set extrapolations, based on the cardinal number X , or additivity assumptions. Final predictions are boldfaced. Uncertainties are given in parentheses.					

An electron-deficient ring, represented by C₆H₆ in our model systems, directs the interacting anion (H⁻, F⁻, and Cl⁻) to a perpendicular arrangement. In contrast, the cation (in our simplest model cases H⁺, Li⁺, and Na⁺) is forced to a co-planar position near the partially negatively charged ring edge. The optimized structures of these complexes are shown in the bottom two panels of Figure 4.

The bottom two panels of Figure 5 provide insight into the actual stabilizing overlaps between the PNBOs of the studied complexes. During the AP_⊥ interaction, as expected,^[61] the anti-bonding orbitals of the C—C bonds of the electron-deficient aromatic ring (*p*-type orbitals of the C atoms) are filled by lone-pair electrons of the anion. In contrast, the CP_{||} interaction occurs between the overlapping (both *s*- and *p*-type) lone pairs of the F atoms of hexafluoro-benzene and the vacant valence-shell orbitals of the cation.

Finally, we note that in “real” peptides and proteins the “gas-phase” model structures computed accurately as part of this study may be altered by environmental effects, such as solvation or an apolar surrounding medium in the inner part of a protein, as well as by cooperativity with other weak interactions stabilizing the given macromolecule.^[44]

Interaction Energies

Accurate interaction energies have been determined in this study using the FPA technique. Two characteristic examples of a relative-energy estimation based on the FPA scheme, concerning

the C₆H₆ + Na⁺ CP_⊥ and C₆H₆ + Cl⁻ AP_{||} complexes, are given in Table 1. Extensive FPA tables are reported in the Supporting Information for each non-covalent IAR complex studied in this article (Supporting Information Tables S2-S19). Benchmark stabilization energies obtained for all four types of IAR interactions characterizing the studied complexes are presented in Table 2.

For the small cationic complexes, including the Na⁺-C₆H₆ complex shown in Table 1, the HF method provides a reliable estimate of the interaction energy. The MP2 energy increments, denoted by $\delta[\text{MP2}]$ in Table 1, are usually small positive values, for the Na⁺-C₆H₆ complex; for example, it is +1.39 kcal mol⁻¹ at the CBS limit. The CC energy increments $\delta[\text{CCSD}]$ and $\delta[\text{CCSD(T)}]$ are even smaller, they are -0.22 and +0.04 kcal mol⁻¹, respectively.

In the cationic cases the correction of the interaction energies with the core-correlation effect is sizeable, for the Na⁺-C₆H₆ complex it is -2.21 kcal mol⁻¹, as cations are treated as having no valence-electrons in FC computations.

In contrast, for the anionic complexes, including the Cl⁻-C₆H₆ complex shown in Table 1, the HF method accounts only for slightly more than half of the overall interaction (stabilization) energy. This result points toward the importance of electron correlation, it appears to be essential in describing long-range anionic interactions. For the anionic complexes, the MP2 increments are always negative and tend to have almost the same absolute value as the HF stabilization energy, between -4 and -8 kcal mol⁻¹. The F⁻-containing complexes are exceptions, there the HF method seems to be more capable of describing correctly the magnitude of the

Table 2. Interaction energies (ΔE_{FPA}), in kcal mol⁻¹, characterizing the four interaction types of ion–aromatic-ring complexes, computed with the focal-point analysis (FPA) technique (see the Supporting Information for detailed FPA tables).

CP _⊥			AP			
Molecule	ion	ΔE_{FPA}	Molecule	ion	ΔE_{FPA} (bifurcated)	ΔE_{FPA} (linear)
C ₆ H ₆	H ⁺	-177.46(34)	C ₆ H ₆	H ⁻	-6.25(4)	-6.23(3)
	Li ⁺	-36.71(30)		F ⁻	-13.88(10)	-15.56(6)
	Na ⁺	-23.42(25)		Cl ⁻	-8.54(15)	-8.02(16)
AP _⊥			CP			
Molecule	ion	ΔE_{FPA}	Molecule	ion	ΔE_{FPA} (bifurcated)	ΔE_{FPA} (linear)
C ₆ F ₆	H ⁻	-14.41(14)	C ₆ F ₆	H ⁺	-115.72(28)	-118.89(22)
	F ⁻	-20.47(15)		Li ⁺	-21.67(10)	-16.39(8)
	Cl ⁻	-14.69(30)		Na ⁺	-13.32(10)	-9.13(10)

Binding energies of the odd covalent complexes corresponding to proton affinities of C₆H₆ and C₆F₆ are given in italics. Isoelectronic ionic systems corresponding to C₆H₆/C₆F₆ rings are printed boldfaced.

interaction, with a negative MP2 increment only about a quarter of the HF contribution. For the anionic complexes, the singles and doubles CC increments are positive, 0.2–2.6 kcal mol⁻¹ (with the sole exception of the F⁻-C₆F₆ complex), while for the triples (T) excitations the increments are negative, -0.7 to -1.6 kcal mol⁻¹.

Corrections of the interaction energies due to ZPVE are in general within the margin of the uncertainty of the final stabilization energy. The Na⁺- and Li⁺-containing complexes are exceptions but this has no consequence on the accuracy of the stabilization energies.

The small estimated uncertainty of the FPA relative energies, 0.2–0.5 kcal mol⁻¹, comes from several sources. The uncertainty of the HF interaction energy, extrapolated to the CBS limit ($E_{\text{CBS}}^{\text{HF}}$),^[62] is usually only 0.01–0.02 kcal mol⁻¹, as convergence of the HF energy with respect to the cardinal number, *X*, of the applied correlation-consistent basis set family is fast. Convergence of the correlation energy increments, denoted by δ in Table 1, is less rapid. For small cationic complexes, the uncertainty is dominated by the harmonic approximation to the ZPVEs and the uncertainty of the “core” corrections. For the anionic systems, the uncertainty originates mainly from the uncertainty of the CCSD and CCSD(T) relative energy increments. Based on the convergence behavior of the coupled cluster series, post-CCSD(T) corrections are estimated to be negligible, less than 0.1 kcal mol⁻¹, for all cases studied. Overall, the FPA results of this study are the most accurate interaction-energy values established for these IAR complexes and serve as benchmark values for the rest of this and future studies.

It is apparent from our detailed electronic structure computations that all of the IAR interactions are attractive. Nevertheless, there are significant differences in the binding energies. The strongest non-covalent IAR interaction is the CP_⊥ one with binding energies in the range of 23 to 37 kcal mol⁻¹. This is followed by the somewhat weaker AP_⊥ interaction, with stabilization energies between 14 and 21 kcal mol⁻¹. Then come the two interactions resulting in a co-planar structure, the CP_{||} (9–22 kcal mol⁻¹) and the AP_{||} interactions (6–16 kcal mol⁻¹). As expected, with increasing ion size the interactions become noticeably weaker.

This observation implies that dispersion plays only a minor role in these mainly electrostatic interactions.

By comparing the interaction energies of isoelectronic systems (for example, F⁻ or Na⁺ interacting with either C₆H₆ or C₆F₆), we can gain insight into the quantitative energy difference between interactions leading to co-planar and perpendicular structures. Furthermore, the binding energies of the Na⁺ + C₆H₆ and F⁻ + C₆F₆ complexes in the perpendicular arrangement are comparable in magnitude (~21 kcal mol⁻¹), which supports the finding of Kim et al.^[30] regarding the similar strength of the perpendicular CP_⊥ and AP_⊥ interactions. The corresponding edge-wise interaction is stronger for the F⁻ + C₆F₆ complex than for the Na⁺ + C₆F₆ complex, in both the linear and the bifurcated arrangements. This difference arises from the shorter equilibrium distance between the fluoride ion and the benzene ring with respect to the Na⁺-C₆F₆ ring distance (see Supporting Information Table S1); this short distance allows the anion to polarize and overlap with the antibonding C–H orbitals of the aromatic ring more effectively.

Overall, when isoelectronic systems are considered, we find that when the IAR interaction results in a coplanar structure (CP_{||} and AP_{||}), the stabilization energies are ~60% less than those corresponding to a perpendicular structure. Of course, gas-phase interaction energies may also be affected by substituent effects or cooperativity with other NCI, such as H-bonding, π - π stacking, or other van der Waals forces.^[42,44]

Toward Biomolecular Complexes

Characteristic interactions

To mimic IAR interactions in proteins better, we chose to investigate more complex models, as well, where the ions interacting with the aromatic C₆H₆ or C₆F₆ rings are polyatomic moieties: the larger anions chosen are HCOO⁻ and CH₃COO⁻, while the larger cations selected are NH₄⁺ and CH₃NH₃⁺. The computed equilibrium structures of these complexes, as indicated in Figure 6 and Supporting Information Figure S5, are consistent with the ion-quadrupole interaction picture. Thus, these more complex pairs fit perfectly into the

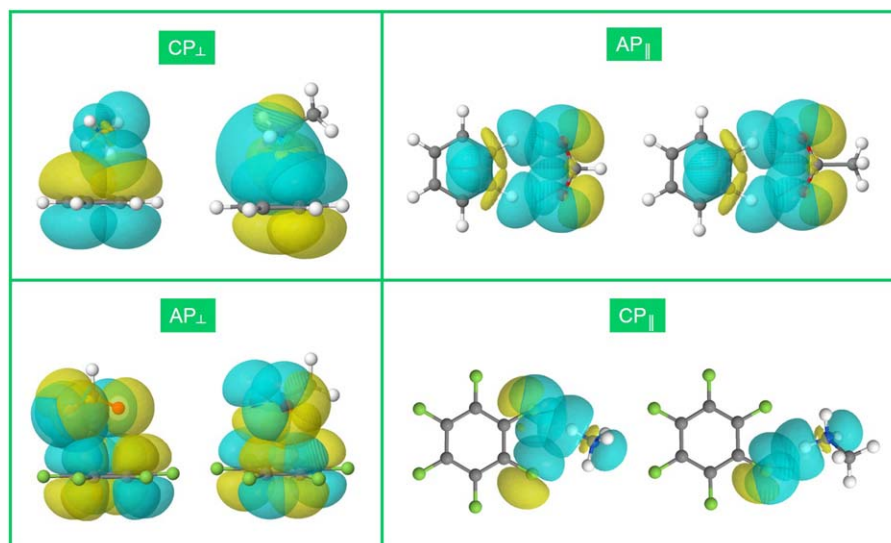


Figure 6. Stabilizing pre-orthogonal natural bond orbital overlaps characterizing the $X^- + C_6H_6$, $M^+ + C_6H_6$, $X^- + C_6F_6$, and $M^+ + C_6F_6$, with $X = HCOO^-$, CH_3COO^- and $M = NH_4^+$, $CH_3NH_3^+$, systems, grouped according to the four ion-aromatic-ring interaction types. [Color figure can be viewed at wileyonlinelibrary.com]

proposed classification of IAR interactions. As expected for an AP_{\parallel} complex, both the formate and the acetate ions form H-bonds between the two oxygen atoms of the ion and the two nearest hydrogen atoms of benzene and adopt a co-planar arrangement with respect to the aromatic ring. In the AP_{\perp} structures, the two ions are positioned above the electron-deficient ring, with the oxygen atoms interacting with the partially positively charged face of the ring. The cations NH_4^+ and $CH_3NH_3^+$ are found above the partially negatively charged π -electron cloud of benzene, forming a CP_{\perp} complex, whereas in both CP_{\parallel} complexes they form an H-bond with one of the fluorine atoms on the ring edge of C_6F_6 .

According to a NBO analysis of these complexes, the interactions are very similar to those observed for the simpler systems; however, somewhat more complex orbital overlap structures evolve here, as shown in Figure 6. In the case of the AP_{\parallel} interaction, the antibonding orbital of the C—H bond of the benzene ring receives electrons from the anion; the lone pairs of the O atoms and also from the bonding orbitals of the C—O bonds of $HCOO^-$ and CH_3COO^- . The reverse holds for the CP_{\parallel} complexes, where the electrons of the lone pairs of the F atoms of hexafluoro-benzene delocalize into the anti-bonding orbitals of the N—H bonds of the NH_4^+ and $CH_3NH_3^+$ cations. In the perpendicular arrangement of the CP_{\perp} systems these cations also use their anti-bonding orbitals, as proposed for aryl amines,^[63] drawing charge from the aromatic π system. For the AP_{\perp} system formed by C_6F_6 and the $HCOO^-$ and CH_3COO^- ions, the bonding orbitals of the ions donate electrons to the π -system of the ring.

Accurate interaction energies

The binding energy trends observed for IAR complexes containing a monatomic ion are reproduced in the larger complexes containing polyatomic ions (see Table 3). Again, the strongest

interaction occurs between the CP_{\perp} complexes of (NH_4^+ , $CH_3NH_3^+$) and C_6H_6 (with a stabilization energy of ~ 17 kcal mol⁻¹), followed by the slightly less favorable AP_{\perp} complexes of ($HCOO^-$, CH_3COO^-) and C_6F_6 (~ 16 kcal mol⁻¹), and the two co-planar arrangements of ($HCOO^-$, CH_3COO^-) with C_6H_6 (~ 10 kcal mol⁻¹), and (NH_4^+ , $CH_3NH_3^+$) with C_6F_6 (~ 9 kcal mol⁻¹). The substantial difference in the binding energy of the co-planar and the perpendicular arrangements is the result of the bulkiness of the polyatomic ion. In the edge-wise orientation, the attractive electrostatic interaction is weakened by the van der Waals (vdW) repulsion of the approaching atoms, whereas in the point-to-plane structure vdW forces play only a minor role, the ion can move closer to the aromatic ring.

Testing density functional theory

In the previous sections, FPA and NBO analyses have provided insight into the main characteristics of the IAR interaction, either quantitatively or qualitatively. When studying larger organic and biomolecules, we must replace the expensive (but accurate) FPA technique with a reliable (but computationally much less demanding) electronic structure method. DFT is an obvious choice. However, hallmarks of DFT also include the

Table 3. FPA interaction energies, in kcal mol⁻¹, of ion-aromatic-ring complexes containing polyatomic ions.

Molecule	CP _⊥		AP _∥	
	Ion	ΔE_{FPA}	Ion	ΔE_{FPA}
C ₆ H ₆	NH ₄ ⁺	-17.82(17)	HCOO ⁻	-10.20(10)
	CH ₃ NH ₃ ⁺	-16.78(31)	CH ₃ COO ⁻	-10.66(10)
C ₆ F ₆	AP _⊥		CP _∥	
	HCOO ⁻	-16.77(21)	NH ₄ ⁺	-9.36(9)
	CH ₃ COO ⁻	-15.61(38)	CH ₃ NH ₃ ⁺	-8.64(14)

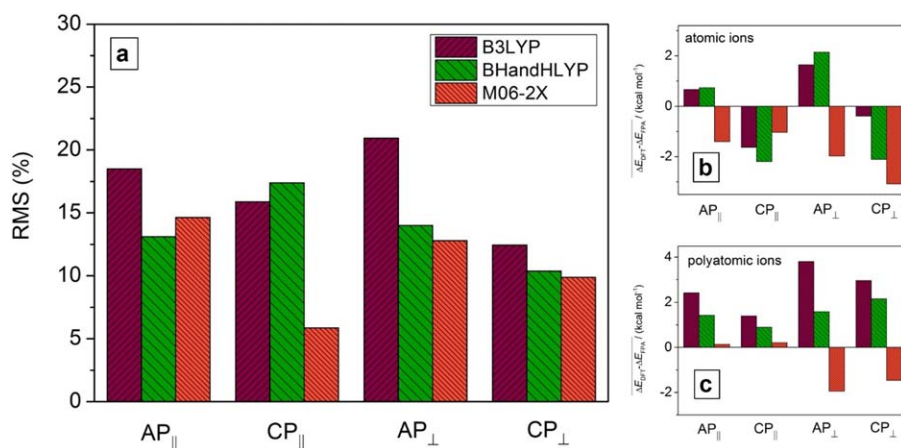


Figure 7. a) (left-hand side): Root mean square (RMS) deviations of the DFT and FPA energy values, given as a fractional difference (%) with respect to the benchmark FPA interaction energies for each type of ion–aromatic-ring interactions, including both atomic and polyatomic ions and three DFT functionals (B3LYP, BHandHLYP, and M06-2X). b) (top right): Average deviations of DFT interaction energies from FPA results for ion–aromatic-ring complexes containing atomic ions, in kcal mol⁻¹. c) (bottom right): Average deviations of DFT interaction energies from FPA results for ion–aromatic-ring complexes containing polyatomic ions, in kcal mol⁻¹. This figure is based on data listed in Supporting Information Tables S30–S32. [Color figure can be viewed at wileyonlinelibrary.com]

lack of a systematic improvement of the results and the lack of a systematic way to estimate uncertainties. Therefore, a given DFT functional should always be tested for a given interaction type before it is applied. The benchmark-quality FPA structures and relative energies serve as perfect references for this test.

To inspect the performance of DFT methods for IAR systems, we selected three widely used DFT functionals and carried out geometry optimizations and stabilization energy computations. We selected the BHandHLYP functional,^[64] developed for anionic systems featuring long-range interactions, the M06-2X functional,^[65] developed for systems characterized by NCI, and the B3LYP^[66] functional.

For the complexes involving atomic ions, we mostly found the same minima and transition states with DFT as with DF-MP2. Nevertheless, a few exceptions, listed in the Supporting Information, must be noted. It is important to emphasize that for the larger systems involving polyatomic ions basically the same minima were obtained during the DFT and DF-MP2 optimizations. This suggests that for larger molecules the selected DFT methods reproduce correctly the structural preferences of IAR systems.

As to the relative energies obtained from DFT computations, an average deviation of 10–15%, depending strongly on the interaction type and the ion, is observed from the corresponding FPA values; for details see Supporting Information Tables S22 to S32. The covalently-bonded systems are excluded from the analysis. Figure 7a presents the root mean square (rms) deviations of the differences (in %) between the DFT and the FPA interaction energies for each IAR interaction type. The observed deviations involve both over- and underestimations of the FPA interaction energies. As seen in Figures 7b and 7c, the M06-2X functional tends to overestimate the interaction energies, whereas the B3LYP and BHandHLYP functionals tend to underestimate them. The M06-2X functional performs better in the case of the larger systems, possibly due to the fact that it includes a dispersion correction. Dispersions are expected to

play an important role as the size of the studied (bio)systems increases.

Figure 7 suggests that among the DFT functionals tested the M06-2X functional usually performs the best. M06-2X performs especially well in the case of complexes containing polyatomic ions, where it reproduces the FPA energies with absolute differences less than 0.5 kcal mol⁻¹ in the case of AP_{||} and CP_{||} interactions, while the differences are less than 2.0 kcal mol⁻¹ for the perpendicular arrangements. It is also important to observe that the performance of the BHandHLYP functional, developed for long-range interactions, is not better than that of the other two functionals. The B3LYP functional, lacking a dispersion correction, is seemingly not suitable to describe IAR interactions, the rms deviations are always larger than 12% and reach even 20%. To conclude, if one would like to obtain chemically accurate interaction energies, meaning an error less than 1 kcal mol⁻¹, for non-covalently-bonded IAR systems, it is still recommended to use *ab initio* methods describing accurately the electron correlation and possibly the FPA scheme to get accurate relative energies with reasonable uncertainties. Nevertheless, to achieve a qualitative understanding of interaction energy trends in IAR systems, the use of, for example, the M06-2X DFT functional would also be appropriate, as it does not change the energy order of the four basic interaction types.

A comparison similar to Figure 7 is presented in Figure S7 of the Supporting Information between MP2 (energies are taken from the FPA scheme (MP2/aug-cc-pVTZ) and improved with ZPVE correction) and DFT methods, usually applied to larger systems. This comparison suggests that, as expected, the M06-2X results are the closest to those of MP2. However, on average a 10–12% rms deviation is observed even in this case. The agreement is considerably better in the case of large IAR complexes. The performance of MP2 compared to FPA is also plotted in Supporting Information Figure S8, which shows a constant 8–10% rms deviation, independent of the IAR interaction type. In conclusion, MP2 performs better than DFT with

respect to the benchmark FPA results. However, in the case of the M06-2X functional, MP2 and DFT give results of similar quality, with a 10% deviation with respect to the benchmark-quality FPA energies.

Conclusions

Structures and relative energies of several model complexes, mimicking NCI of aromatic rings with positively and negatively charged moieties, have been studied, where electron-rich (modeled by benzene) and electron-deficient (modeled by hexafluoro-benzene) aromatic rings interact either with cations (H^+ , Li^+ , Na^+ , NH_4^+ , and $CH_3NH_3^+$) or with anions (H^- , F^- , Cl^- , $HCOO^-$, and CH_3COO^-). Our quantum chemical modeling study reaffirms that electrostatic, in particular quadrupole-charge, interactions govern the structural preferences of IAR systems. The quadrupole-charge interactions lead to two fundamentally distinct structural arrangements for the cations and the anions: the ions show either a perpendicular or a co-planar arrangement with respect to the plane of the aromatic ring. Nevertheless, in real systems affected by environmental effects, such as solvation and an interplay among several types of interactions, the orientations may change appreciably.

An exploratory database search using the PDB and the CSD suggests that these IAR interaction types are not only present in proteins but also in small organic complexes. Thus, it is not only the protein scaffold which provides the necessary flexibility for the IAR interactions to take place, but, due to the associated relatively large interaction energies, they also occur in small molecular complexes having much less structural flexibility.

Based on a NBO analysis, we identified the essential localized orbital overlaps that stabilize the preferred perpendicular or co-planar structures. The findings are in line with chemical intuition. As to the case of an electron-rich π system, a lone pair of an anion forms H-bond(s) with the C–H anti-bonding orbitals of the benzene ring and this way a co-planar structure is adopted, while a cation fills its vacant valence-shell orbitals by accepting electrons from the π -system of the aromatic ring. In clear contrast, in the case of the electron-deficient ring the anion is positioned above the aromatic ring, thereby donating electrons to the anti-bonding π -orbitals of the ring, whereas the cation is found in a co-planar arrangement with the ring plane and receives electrons from the lone pair of the nearest fluorine atoms of the hexafluoro-benzene ring.

In line with this physical picture, we propose to use the following four interaction types during the discussion of the interaction between ions and aromatic rings: perpendicular cation- π (CP_{\perp} , called cation- π in the literature), co-planar cation- π (CP_{\parallel}), perpendicular anion- π (AP_{\perp} , called anion- π in the literature), and co-planar anion- π (AP_{\parallel}). Based on highly accurate interaction energies obtained from a FPA study, we show that all four types of IAR interactions are characterized by significant stabilization energies.

As a step toward a comprehensive study of larger biological systems, larger, polyatomic-ion-containing IAR complexes have also been studied. The FPA stabilization energies corresponding to these reference systems serve as benchmark values helping

to judge the performance of DFT computations. From the three chosen DFT functionals, B3LYP, BHandHLYP, and M06-2X, the M06-2X functional appears to reproduce most reliably the benchmark FPA interaction energies. When comparing the two electronic structure methods applicable for large systems, DFT and MP2, it turns out that MP2 usually performs better than DFT (the reference energies are those provided by the highly accurate FPA technique); however, the M06-2X functional provides results of quality similar to that of MP2. Thus, we recommend this functional for future use in studying IAR interactions in peptides, proteins or larger molecular complexes.

The IAR interactions appear to have stabilization energies comparable to other non-covalent stabilizing forces (for example, H-bonds and salt bridges). In the model systems studied, the CP_{\perp} , AP_{\perp} , CP_{\parallel} and AP_{\parallel} interaction types are characterized by stabilization energies of 23–37, 14–21, 9–22, and 6–16 kcal mol⁻¹, respectively. The aqueous medium surrounding proteins in real systems reduces these substantial interaction energies by up to an order of magnitude. Thus, these IAR contacts are supposed to stabilize especially the inner, buried parts of a folded protein. With the clear characteristics of IAR donor-acceptor overlapping patterns in mind, obtained from a NBO analysis, tools may become available in the future for fine-tuning these sensitive interactions when designing molecular folds and complexes.

Acknowledgment

This investigation was performed as part of a feasibility study leading to a grant application (VEKOP).

Keywords: non-covalent interaction · focal-point analysis of interaction energies · ion–aromatic-ring interaction · natural bond orbital analysis

How to cite this article: D. Papp, P. Rovó, I. Jákli, A. G. Császár, A. Perczel *J. Comput. Chem.* **2017**, *38*, 1762–1773. DOI: 10.1002/jcc.24816

 Additional Supporting Information may be found in the online version of this article.

- [1] J. Sunner, K. Nishizawa, P. Kebarle, *J. Phys. Chem.* **1981**, *85*, 1814.
- [2] J. C. Ma, D. A. Dougherty, *Chem. Rev.* **1997**, *97*, 1303.
- [3] J. P. Gollivan, D. A. Dougherty, *Proc. Natl. Acad. Sci. USA* **1999**, *96*, 9459.
- [4] N. Zacharias, D. A. Dougherty, *Trends. Pharmacol. Sci.* **2002**, *23*, 281.
- [5] D. Quinonero, C. Garau, C. Rotger, A. Frontera, P. Ballester, A. Costa, P. M. Deya, *Angew. Chem. Int. Ed.* **2002**, *41*, 3389.
- [6] B. L. Schottel, H. T. Chifotides, K. R. Dunbar, *Chem. Soc. Rev.* **2008**, *37*, 68.
- [7] T. J. Mooibroek, C. A. Black, P. Gamez, J. Reedijk, *Cryst. Growth. Des.* **2008**, *8*, 1082.
- [8] C. Caltagirone, P. A. Gale, *Chem. Soc. Rev.* **2009**, *38*, 520.
- [9] R. E. Dawson, A. Hennig, D. P. Weimann, D. Emery, V. Ravikumar, J. Montenegro, T. Takeuchi, S. Gabutti, M. Mayor, J. Mareda, C. A. Schalley, S. Matile, *Nat. Chem.* **2010**, *2*, 533.
- [10] A. Frontera, P. Gamez, M. Mascal, T. J. Mooibroek, J. Reedijk, *Angew. Chem. Int. Ed.* **2011**, *50*, 9564.
- [11] A. Robertazzi, F. Krull, W. E. Knapp, P. Gamez, *Crystengcomm* **2011**, *13*, 3293.

- [12] K. D. Daze, F. Hof, *Acc. Chem. Res.* **2013**, *46*, 937.
- [13] N. Z. Xie, Q. S. Du, J. X. Li, R. B. Huang, *PLoS One* **2015**, *10*, e0137113.
- [14] H. Zheng, K. Comeforo, J. M. Gao, *J. Am. Chem. Soc.* **2009**, *131*, 18.
- [15] T. W. Craven, M. Chuo, N. J. Traaseth, R. Bonneau, K. Kirshenbaum, *J. Am. Chem. Soc.* **2016**, *138*, 1543.
- [16] Y. Z. Liu, K. Yuan, L. L. Lv, Y. C. Zhu, Z. Yuan, *J. Phys. Chem. A* **2015**, *119*, 5842.
- [17] M. J. Chmielewski, M. Charon, J. Jurczak, *Org. Lett.* **2004**, *6*, 3501.
- [18] D. A. Dougherty, *Science* **1996**, *271*, 163.
- [19] A. S. Mahadevi, G. N. Sastry, *Chem. Rev.* **2013**, *113*, 2100.
- [20] W. G. Zhong, J. P. Gallivan, Y. O. Zhang, L. T. Li, H. A. Lester, D. A. Dougherty, *Proc. Natl. Acad. Sci. USA* **1998**, *95*, 12088.
- [21] M. R. Battaglia, A. D. Buckingham, J. H. Williams, *Chem. Phys. Lett.* **1981**, *78*, 421.
- [22] S. Mecozzi, A. P. West, D. A. Dougherty, *Proc. Natl. Acad. Sci. USA* **1996**, *93*, 10566.
- [23] S. Mecozzi, A. P. West, D. A. Dougherty, *J. Am. Chem. Soc.* **1996**, *118*, 2307.
- [24] C. Garau, A. Frontera, D. Quinonero, P. Ballester, A. Costa, P. M. Deya, *J. Phys. Chem. A* **2004**, *108*, 9423.
- [25] A. S. Reddy, G. N. Sastry, *J. Phys. Chem. A* **2005**, *109*, 8893.
- [26] A. Clements, M. Lewis, *J. Phys. Chem. A* **2006**, *110*, 12705.
- [27] O. B. Berryman, F. Hof, M. J. Hynes, D. W. Johnson, *Chem. Commun.* **2006**, 506.
- [28] I. Alkorta, I. Rozas, J. Elguero, *J. Am. Chem. Soc.* **2002**, *124*, 8593.
- [29] M. Mascal, A. Armstrong, M. D. Bartberger, *J. Am. Chem. Soc.* **2002**, *124*, 6274.
- [30] D. Kim, P. Tarakeshwar, K. S. Kim, *J. Phys. Chem. A* **2004**, *108*, 1250.
- [31] P. D. Mezei, G. I. Csonka, A. Ruzsinszky, J. Sun, *J. Chem. Theory Comput.* **2015**, *11*, 360.
- [32] M. R. Jackson, R. Beahm, S. Duvvuru, C. Narasimhan, J. Wu, H. N. Wang, V. M. Philip, R. J. Hinde, E. E. Howell, *J. Phys. Chem. B* **2007**, *111*, 8242.
- [33] V. Philip, J. Harris, R. Adams, D. Nguyen, J. Spiers, J. Baudry, E. E. Howell, R. J. Hinde, *Biochemistry* **2011**, *50*, 2939.
- [34] J. P. Schwans, F. Sunden, J. K. Lassila, A. Gonzalez, Y. Tsai, D. Herschlag, *Proc. Natl. Acad. Sci. USA* **2013**, *110*, 11308.
- [35] D. D. Jenkins, J. B. Harris, E. E. Howell, R. J. Hinde, J. Baudry, *J. Comput. Chem.* **2013**, *34*, 518.
- [36] Available at: <http://www.rcsb.org/pdb/home/home.do>, accessed on January 19, **2017**.
- [37] Available at: <https://www.ccdc.cam.ac.uk/>, accessed on January 19, **2017**.
- [38] W. D. Allen, A. L. L. East, A. G. Császár, In *Structures and Conformations of Non-Rigid Molecules*, J. Laane, M. Dakkouri, B. van der Veken, H. Oberhammer, Eds.; Kluwer: Dordrecht, The Netherlands, **1993**; pp. 343–373.
- [39] A. G. Császár, W. D. Allen, H. F. Schaefer, *J. Chem. Phys.* **1998**, *108*, 9751.
- [40] A. S. Reddy, G. M. Sastry, G. N. Sastry, *Proteins Struct. Funct. Bioinform.* **2007**, *67*, 1179.
- [41] Available at: <http://www.ccdc.cam.ac.uk/Solutions/CSDSystem/Pages/ConQuest.aspx>, accessed on January 19, **2017**.
- [42] S. E. Wheeler, K. N. Houk, *J. Am. Chem. Soc.* **2009**, *131*, 3126.
- [43] L. Nogueiras-Nieto, C. Alvarez-Lorenzo, I. Sandez-Macho, A. Concheiro, F. J. Otero-Espinar, *J. Phys. Chem. B* **2009**, *113*, 2773.
- [44] A. S. Mahadevi, G. N. Sastry, *Chem. Rev.* **2016**, *116*, 2775.
- [45] F. R. Manby, *J. Chem. Phys.* **2003**, *119*, 4607.
- [46] H. J. Werner, F. R. Manby, P. J. Knowles, *J. Chem. Phys.* **2003**, *118*, 8149.
- [47] U. Bozkaya, *J. Chem. Phys.* **2014**, *141*, 124108.
- [48] T. H. Dunning, *J. Chem. Phys.* **1989**, *90*, 1007.
- [49] A. G. Császár, A. Perczel, *Prog. Biophys. Mol. Biol.* **1999**, *71*, 243.
- [50] J. J. Wilke, M. C. Lind, H. F. Schaefer, A. G. Császár, W. D. Allen, *J. Chem. Theory Comput.* **2009**, *5*, 1511.
- [51] T. Szidarovszky, G. Czakó, A. G. Császár, *Mol. Phys.* **2009**, *107*, 761.
- [52] F. Pollreis, Á. Gömör, G. Schlosser, K. Vékey, I. Solt, A. G. Császár, *Chem. Eur. J.* **2005**, *11*, 5908.
- [53] M. S. Deleuze, L. Claes, E. S. Kryachko, J. P. Francois, *J. Chem. Phys.* **2003**, *119*, 3106.
- [54] H. J. Werner, P. J. Knowles, G. Knizia, F. R. Manby, M. Schütz, P. Celani, W. Györffy, D. Kats, T. Korona, R. Lindh, A. Mitrushenkov, G. Rauhut, K. R. Shamasundar, T. B. Adler, R. D. Amos, A. Bernhardsson, A. Berning, D. L. Cooper, M. J. O. Deegan, A. J. Dobbyn, F. Eckert, E. Goll, C. Hampel, A. Hesselmann, G. Hetzer, T. Hrenar, G. Jansen, C. Köppl, Y. Liu, A. W. Lloyd, R. A. Mata, A. J. May, S. J. McNicholas, W. Meyer, M. E. Mura, A. Nicklaß, D. P. O'Neill, P. Palmieri, D. Peng, K. Pflüger, R. Pitzer, M. Reiher, T. Shiozaki, H. Stoll, A. J. Stone, R. Tarroni, T. Thorsteinsson, M. Wang, MOLPRO, A Package of ab Initio Programs, version 2012.1. Available at: <http://www.molpro.net>, accessed on January 19, **2017**.
- [55] M. J. Frisch, G. W. Trucks, H. B. Schlegel, G. E. Scuseria, M. A. Robb, J. R. Cheeseman, G. Scalmani, V. Barone, B. Mennucci, G. A. Petersson, H. Nakatsuji, M. Caricato, X. Li, H. P. Hratchian, A. F. Izmaylov, J. Bloino, G. Zheng, J. L. Sonnenberg, M. Hada, M. Ehara, K. Toyota, R. Fukuda, J. Hasegawa, M. Ishida, T. Nakajima, Y. Honda, O. Kitao, H. Nakai, T. Vreven, J. A. Montgomery, Jr., J. E. Peralta, F. Ogliaro, M. Bearpark, J. J. Heyd, E. Brothers, K. N. Kudin, V. N. Staroverov, R. Kobayashi, J. Normand, K. Raghavachari, A. Rendell, J. C. Burant, S. S. Iyengar, J. Tomasi, M. Cossi, N. Rega, J. M. Millam, M. Klene, J. E. Knox, J. B. Cross, V. Bakken, C. Adamo, J. Jaramillo, R. Gomperts, R. E. Stratmann, O. Yazyev, A. J. Austin, R. Cammi, C. Pomelli, J. W. Ochterski, R. L. Martin, K. Morokuma, V. G. Zakrzewski, G. A. Voth, P. Salvador, J. J. Dannenberg, S. Dapprich, A. D. Daniels, Ö. Farkas, J. B. Foresman, J. V. Ortiz, J. Cioslowski, D. J. Fox, *Gaussian 09, Revision C.01*; Gaussian, Inc.: Wallingford, CT, **2010**.
- [56] G. Tarczay, A. G. Császár, W. Klopper, H. M. Quiney, *Mol. Phys.* **2001**, *99*, 1769.
- [57] H. M. Jaeger, H. F. Schaefer, III, J. Demaison, A. G. Császár, W. D. Allen, *J. Chem. Theory Comput.* **2010**, *6*, 3066.
- [58] F. Weinhold, *J. Comput. Chem.* **2012**, *33*, 2363.
- [59] Available at: <http://nbo6.chem.wisc.edu/>, accessed on January 19, **2017**.
- [60] A. E. Reed, F. Weinhold, *J. Chem. Phys.* **1985**, *83*, 1736.
- [61] A. Ebrahimi, M. Habibi, O. Sayyadi, *J. Mol. Struct. (Theochem)* **2008**, *859*, 46.
- [62] G. Tasi, A. G. Császár, *Chem. Phys. Lett.* **2007**, *438*, 139.
- [63] S. Kheirjou, A. Fattahi, M. M. Hashemi, *Comput. Theor. Chem.* **2014**, *1036*, 51.
- [64] A. D. Becke, *J. Chem. Phys.* **1993**, *98*, 1372.
- [65] Y. Zhao, D. G. Truhlar, *Theor. Chem. Acc.* **2008**, *120*, 215.
- [66] P. J. Stephens, F. J. Devlin, C. F. Chabalowski, M. J. Frisch, *J. Phys. Chem.* **1994**, *98*, 11623.

Received: 28 January 2017
Revised: 5 April 2017
Accepted: 6 April 2017
Published online on 10 May 2017